J. Phys. B: At. Mol. Opt. Phys. **29** (1996) 2775–2796. Printed in the UK

Positron–hydrogen and positronium–proton scattering at intermediate and high energies

Kuru Ratnavelu†§, Jim Mitroy‡ and Andris T Stelbovics†

† Centre for Atomic, Molecular and Surface Physics, School of Mathematical and Physical Sciences, Murdoch University, Perth 6150, Australia

‡ Faculty of Science, Northern Territory University, Casuarina, Northern Territory 0909, Australia

Received 29 August 1995

Abstract. Positron scattering from atomic hydrogen is studied at energies ranging from 4 to 100 Ryd using the close-coupling approach and cross sections from both the e^+–H and Ps–p entrance channels are reported in a basis comprising 1s, 2s and 2p states of the hydrogen and positronium atoms. Comparative studies with widely used approximation methods such as the first Born, unitarized Born and second Born approximations are presented. With the exception of elastic scattering for the Ps(1s)–p entrance channel, it was found that on-shell approximations such as the first Born and the unitarized Born approximations are reasonably accurate for collisions not involving particle transfer provided the energy is sufficiently high. Rearrangement collisions on the other hand are dominated by off-the-energy-shell scattering and the accurate approximation at high energies is the second Born approximation. Further, the effects of positronium channels on the direct reactions are investigated and we conclude that the positronium formation channels can be omitted for energies greater than 20 Ryd. Elastic scattering in the Ps(1s)–p entrance channel is seen to be unique, the high-energy behaviour of the phase shifts is different from any other quantum system.

1. Introduction

In the last few years there has been a spurt of theoretical studies on positron–hydrogen atom scattering processes. Besides the motivation that it is one of the fundamental three-body systems of atomic physics, one of the main reasons for these calculations has been the recent availability of workstations that are sufficiently fast to handle the complexities inherent in a system that permits a rearrangement collision, namely positronium formation. Furthermore, the concurrent improvement in positron-beam technology has lead to the first generation of experimental measurements for the positron–hydrogen ionization cross section (Spicher *et al* 1990, Sperber *et al* 1992, Jones *et al* 1993), the total reaction cross section (Zhou *et al* 1994) and the positronium-formation cross section (Weber *et al* 1994) and this has provided a further incentive for calculations.

While there have been a number of theoretical studies for the positron–hydrogen system, most of the methods have limitations. For example, the variational calculations (Bhatia *et al* 1971, 1974, Humberston 1982, 1984) were restricted to a few partial waves in the low-energy region below the positronium threshold or in the Ore gap. Calculations using perturbative methods (Basu and Ghosh 1988, Basu *et al* 1976) have also been applied,

§ On sabbatical leave from: Department of Mathematics, University of Malaya, 59100 Kuala Lumpur, Malaysia.

0953-4075/96/132775+22$19.50

but these are only valid at high energies. The close-coupling methods used extensively for electron–atom scattering have also been applied to the study of the positron–hydrogen system. The earliest calculations made use of existing electron–hydrogen close-coupling codes by ignoring the positronium formation channels, and just changing the sign of the incident particle charge.

Intermediate energy calculations of this type include those of Burke *et al* (1963), the pseudostate calculations of Morgan (1982), Walters (1988), an optical potential method based on the coupled-channels formalism (CCOM) by McCarthy and collaborators (Bransden *et al* 1985), the intermediate energy *R*-matrix (IERM) method (Higgins *et al* 1990), and the convergent close-coupling study of Bray and Stelbovics (1994). For a review of earlier studies the readers are referred to Bransden (1969) and Ghosh *et al* (1982).

In 1990, Hewitt *et al* (1990) attempted the first realistic coupled-channels calculations with explicit coupling to the positronium channels in the intermediate energy region. More recently, there have been some 18-state *R*-matrix calculations (McAlinden *et al* 1994, Kernoghan *et al* 1995) that have provided a set of cross sections for both the low and intermediate energy regions. During the same period there was parallel development of the close-coupling method in momentum space by Mitroy (1993a) that was an improvement over the pioneering work of Hewitt *et al* (1990), as a general form for the positronium matrix element was obtained. Further investigations by Mitroy and collaborators on the e^+–H system (Mitroy 1993a, b, 1995, Mitroy and Stelbovics 1994, Mitroy *et al* 1994, Mitroy and Ratnavelu 1995) have culminated in an accurate set of cross sections at low energies (Mitroy 1995). The cross sections from a 21-state close-coupling calculation agree to within a couple of per cent with earlier variational results. The *R*-matrix calculations generally agree with the *T*-matrix calculations at low energies. Therefore, it is now appropriate to focus investigations onto the physics of positron–hydrogen scattering in the intermediate and high-energy regions ranging from 4 to 100 Ryd and this is the motivation for the present work.

The Calcutta group of Ghosh and co-workers have used the close-coupling method to include the positronium channels explicitly and a number of studies in momentum space were done at intermediate energies using a limited basis (Basu *et al* 1976, Basu and Ghosh 1988, Mukherjee *et al* 1990). A recent optical potential calculation of e^+–H has also been done by Ghosh and Darewych (1991). By taking a *P*-space of H(1s) and Ps(1s) states, and a *Q*-space of H(2s) and H(2p) states, they showed that the positronium-formation channel is still important at an energy of 100 eV. Basu and Ghosh (1988) have used the second Born approximation to report cross sections for direct and rearrangement processes at a number of energies. They claimed that the second-order effect is important in modelling the capture cross section at intermediate and high energies. For more details of recent application of perturbative methods, the reader is also referred to the review of Bransden and Noble (1994).

The present work extends the close-coupling method of Mitroy (1993c) to calculate cross sections in the intermediate- and high-energy regime. Further, we study the effects of positronium channels on the direct reactions and the convergence of the perturbative approximation methods (unitarized Born (UBA), first Born (FBA), second Born (SBA)) which are obtained simultaneously as a byproduct of solving the coupled-channels integral equations in momentum-space. Finally we investigate the unique behaviour of the Ps(1s)–p phase-shifts in the high-energy limit. This behaviour is due to the absence of the first-order term in the *T*-matrix element for elastic scattering.

2. Details of calculations

The momentum space Lippmann–Schwinger equations for a positron with momentum $\boldsymbol{k}$ incident on a hydrogen atom in state Ψ_α (atomic units are assumed throughout) are

$$\langle \boldsymbol{k}'\Psi_{\alpha'}|T|\boldsymbol{k}\Psi_\alpha\rangle = \langle \boldsymbol{k}'\Psi_{\alpha'}|V|\boldsymbol{k}\Psi_\alpha\rangle + \sum_{\alpha''}\int \mathrm{d}^3k''\,\frac{\langle \boldsymbol{k}'\Psi_{\alpha'}|V|\boldsymbol{k}''\Psi_{\alpha''}\rangle\langle \boldsymbol{k}''\Psi_{\alpha''}|T|\boldsymbol{k}\Psi_\alpha\rangle}{(E^{(+)} - \varepsilon_{\alpha''} - \frac{1}{2}k''^2)} + \sum_{\beta''}\int \mathrm{d}^3k''\,\frac{\langle \boldsymbol{k}'\Psi_{\alpha'}|V|\boldsymbol{k}''\Phi_{\beta''}\rangle\langle \boldsymbol{k}''\Phi_{\beta''}|T|\boldsymbol{k}\Psi_\alpha\rangle}{(E^{(+)} - \varepsilon_{\beta''} - \frac{1}{4}k''^2)} \tag{1}$$

$$\langle \boldsymbol{k}'\Phi_{\beta'}|T|\boldsymbol{k}\Psi_\alpha\rangle = \langle \boldsymbol{k}'\Phi_{\beta'}|V|\boldsymbol{k}\Psi_\alpha\rangle + \sum_{\alpha''}\int \mathrm{d}^3k''\,\frac{\langle \boldsymbol{k}'\Phi_{\beta'}|V|\boldsymbol{k}''\Psi_{\alpha''}\rangle\langle \boldsymbol{k}''\Psi_{\alpha''}|T|\boldsymbol{k}\Psi_\alpha\rangle}{(E^{(+)} - \varepsilon_{\alpha''} - \frac{1}{2}k''^2)} + \sum_{\beta''}\int \mathrm{d}^3k''\,\frac{\langle \boldsymbol{k}'\Phi_{\beta'}|V|\boldsymbol{k}''\Phi_{\beta''}\rangle\langle \boldsymbol{k}''\Phi_{\beta''}|T|\boldsymbol{k}\Psi_\alpha\rangle}{(E^{(+)} - \varepsilon_{\beta''} - \frac{1}{4}k''^2)} \tag{2}$$

$$\langle \boldsymbol{k}'\Phi_{\beta'}|T|\boldsymbol{k}\Phi_\beta\rangle = \langle \boldsymbol{k}'\Phi_{\beta'}|V|\boldsymbol{k}\Phi_\beta\rangle + \sum_{\alpha''}\int \mathrm{d}^3k''\,\frac{\langle \boldsymbol{k}'\Phi_{\beta'}|V|\boldsymbol{k}''\Psi_{\alpha''}\rangle\langle \boldsymbol{k}''\Psi_{\alpha''}|T|\boldsymbol{k}\Phi_\beta\rangle}{(E^{(+)} - \varepsilon_{\alpha''} - \frac{1}{2}k''^2)} + \sum_{\beta''}\int \mathrm{d}^3k''\,\frac{\langle \boldsymbol{k}'\Phi_{\beta'}|V|\boldsymbol{k}''\Phi_{\beta''}\rangle\langle \boldsymbol{k}''\Phi_{\beta''}|T|\boldsymbol{k}\Phi_\beta\rangle}{(E^{(+)} - \varepsilon_{\beta''} - \frac{1}{4}k''^2)}. \tag{3}$$

In the above equation, Ψ_α and Φ_β refer to the hydrogen and positronium states, respectively. The complete formalism of the close-coupling method in momentum space as applied to the positron–hydrogen system is not discussed here and the reader is referred to the work of Mitroy (1993c).

The calculations reported in this work can be divided into two types: non-perturbative and perturbative. The following non-perturbative calculations were done.

(i) CC(3, 3). This close-coupling calculation includes the hydrogen states H(1s), H(2s), H(2p) together with the positronium states Ps(1s), Ps(2s) and Ps(2p).

(ii) CC(3, 0), CC(0, 3). To investigate the effects of positronium states on the excitation of hydrogen levels, calculations that exclude the positronium channels were performed. These are denoted by CC(3, 0). Similarly, to study the effects of hydrogen states on excitation of positronium levels, calculations that exclude hydrogen channels were performed and are denoted by CC(0, 3). The CC(3, 0) and CC(0, 3) T-matrices were obtained in the same calculation, simply by turning off the rearrangement matrix element connecting the two manifolds of states.

When solving the Lippmann–Schwinger equations in the momentum space representation, it is trivial to obtain perturbative approximations to the full solution of the Lippmann–Schwinger equation. Indeed, these approximate solutions to the full solution of the Lippmann–Schwinger equation are routinely calculated whenever the present program is run. These approximations are

(iii) FBA. These are the first Born approximations to the T-matrix element obtained by setting the integrals in (1)–(3) to zero.

(iv) UBA(3, 3). The UBA is the FBA to the K-matrix which is then used to compute the T-matrix. An alternative interpretation is that the UBA solves the coupled equations to all orders with the restriction that all scattering processes must remain on the energy shell. The UBA is obtained from (1)–(3) by omitting the off-shell part of the channel-free Green functions.

(v) SBA(3, 3). If the T-matrix elements of the right-hand side of (1)–(3) are replaced by the equivalent V-matrix elements, then the resulting T-matrix elements are the second Born approximations.

The numerical techniques that are used to compute the matrix elements and solve the coupled integral equations have been described in McCarthy and Stelbovics (1983, 1994), Mitroy (1993c, 1995) and Mitroy and Ratnavelu (1995) and will not be described in detail here except to note modifications necessary at high energies. In discretizing the kernel, it is important to have sufficiently dense meshes near the on-shell momenta. The main problem in extending the method to higher energies is caused by the on-shell momenta for the positronium channels being about 40% larger than the positron on-shell momenta due to the different masses. This makes it difficult to use bunching transformations to generate a quadrature mesh with a sufficient grid density near both the e^+–H and Ps–p on-shell momenta. Thus instead of using a single Gaussian mesh for these calculations, a five-panel composite mesh was used. The logic behind the mesh is seen by reference to figure 1. The second and fourth regions contain the on-shell momenta of the positron and positronium, respectively. With the increased flexibility inherent in a five-component mesh, it was then relatively straightforward to increase the density of the quadrature mesh close to on-shell momenta. Since the mid-point and the widths of the second and fourth panels were adjustable, it was always possible to distribute the mesh points symmetrically about each of the on-shell momenta. A bunching transformation similar to equation (97) of McCarthy and Stelbovics (1983) was then applied to the second and fourth mesh panels to cluster the quadrature points close to the on-shell momenta in these two panels. The earlier CC(3, 3) calculations of Mitroy and Stelbovics (1994) were restricted to $E < 60$ eV because of the problems of mesh generation at higher energies.

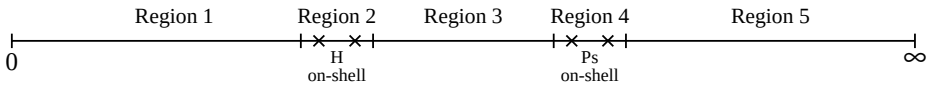

Figure 1. Diagram of a composite Gaussian mesh.

In general, the cross sections for direct transitions not involving electron transfer were stable at all energies. Convergence for these transitions was achieved with a composite mesh with 60 points. However, it was more difficult to achieve convergence for the rearrangement transitions. The difficulties occurred for both the e^+–H(1s) and Ps(1s)–p entrance channels. One difficulty was the rapid decrease of the rearrangement amplitudes with energy when compared to the direct amplitudes. The reason for this arises from the mathematical structure of the rearrangement matrix element which contains terms like $\psi_\alpha(\boldsymbol{k}' - \boldsymbol{k})\phi_\beta(\frac{1}{2}\boldsymbol{k}' - \boldsymbol{k})$. At high energies these terms decrease rapidly because the argument of momentum space wavefunctions gets increasingly larger in the neighbourhood of the on-shell momenta at higher energies. The momentum space wavefunctions are very small except when $k = \frac{1}{2}k'$ and $k = k'$, and neither of these conditions is satisfied by the on-shell momenta in the positron and positronium channels.

In order to obtain converged results, the number of quadrature points in the first interval of the composite mesh had to be steadily increased with energy. This was to ensure that the quadrature mesh was sufficiently dense in the neighbourhood $q = \frac{1}{2}k'$ where k' is the on-shell momentum in the positronium–proton channel. It should be noted that specifics of the mesh automatically ensure a large density of points for the $k = k'$ condition for k or k' on the energy shell. A quadrature mesh containing 68 points was used at 4 Ryd. However, at an energy of 100 Ryd, the mesh had been increased to 92 points to maintain the relative accuracy of the smaller amplitudes. The results were converged to the 1% level at energies $E < 50$ Ryd and about the 5–10% level for $E > 50$ Ryd.

As calculations were performed up to a maximum energy of 100 Ryd, it is clear that a large number of partial waves were required. Due to the time-consuming nature of the calculations, it was not possible to perform fully-close-coupled calculations with explicit inclusion of the rearrangement kernel for 180 partial waves at all energies. The rearrangement matrix elements, in particular, take longer to compute as the angular momentum increases because the algorithm used for computing Legendre functions of the second kind, $Q_l(x)$, becomes increasingly inefficient as l increases. The cross sections were computed with the following succession of approximations each of which had a small effect on the accuracy of the quoted integrated cross sections. For $J \leqslant 22$ the positronium matrix elements were included and the Lippmann–Schwinger equations are solved with no approximation apart from the purely numerical ones inherent in any calculation. For $23 \leqslant J \leqslant 45$, the Lippmann–Schwinger equations are solved but the rearrangement matrix elements were omitted from the calculation. From $46 \leqslant J \leqslant 180$, the UBA(3, 3) model was used to compute the T-matrix elements. For all transitions, the integrated cross section was computed as a discrete sum over individual partial cross sections. A small correction was then made to these cross sections to allow for $J > 180$ ($J > 22$ in the case of rearrangement transitions) by assuming that the partial cross sections scaled as a power series in J.

For the H(1s)–H(2p) cross section, the size of this correction was about 22.5% at $E = 100$ Ryd. The partial-wave summed cross section was $0.090\,893\ \pi a_0^2$ and after extrapolation $0.1114\ \pi a_0^2$. For the H(1s)–Ps(1s) cross section the size of this correction was less than 0.1% at $E = 100$ Ryd. The partial-wave summed cross section was $1.8402^{-7}\ \pi a_0^2$ and after extrapolation $1.8417^{-7}\ \pi a_0^2$. To illustrate the time required for a single energy calculation we note a 68-point CC run with positronium matrix elements up to $J \leqslant 22$ and decoupled CC up to $J = 45$ took about 17 h CPU time on a SUN SS10/52 workstation. The UBA calculations for $46 < J < 180$ took a few minutes. A 92-point calculation increased the CPU time to 32 h.

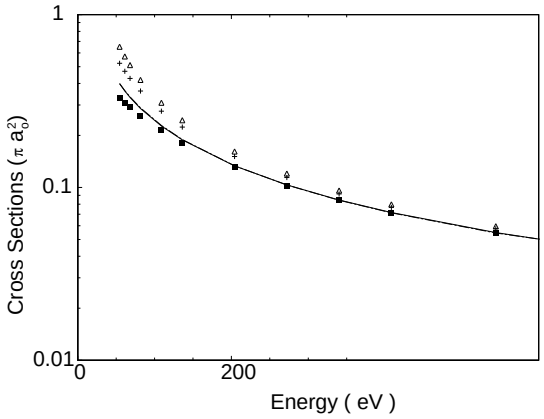

Figure 2. Cross sections (in πa_0^2) for elastic scattering of positrons from the H(1s) state. The cross sections are: CC(3, 3) (——), CC(3, 0) (□), UBA(3, 3) (— · —), FBA (+) and SBA(3, 3) (△).

3. Cross sections for the H(1s) entrance channel

In figures 2–6, the integrated cross sections for elastic scattering, excitation of H(2s) and H(2p) states and positronium formation in the Ps(1s), Ps(2s) and Ps(2p) states are depicted.

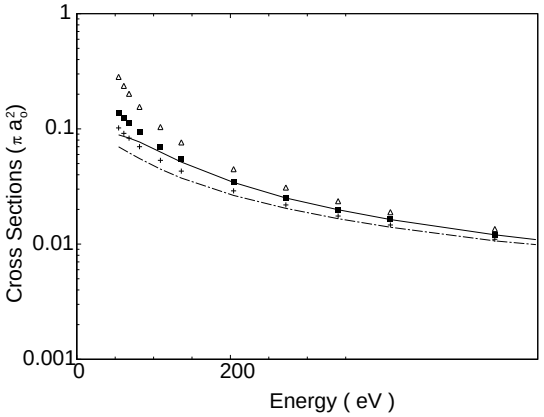

Figure 3. Cross sections (in πa_0^2) for positron excitation of the H(2s) state from the H(1s) entrance channel. The legend is the same as for figure 2.

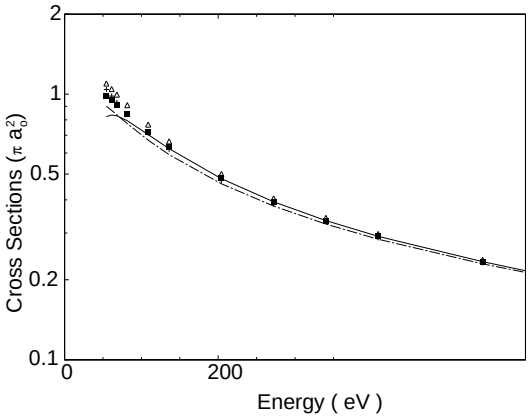

Figure 4. Cross sections (in πa_0^2) for positron excitation of the H(2p) state from the H(1s) entrance channel. The legend is the same as for figure 2.

The integrated cross sections for selected energies are given in tables 1 and 2.

From table 1, it can be seen that the CC(3, 3) and CC(3, 0) cross sections for elastic scattering and excitation of hydrogen differ by 2% at 20 Ryd. At higher energies the agreement between the two sets of cross sections is almost perfect. From this we conclude that the positronium channels exert a negligible influence upon elastic scattering and inelastic scattering within the manifold of hydrogenic initial and final states for energies greater than 20 Ryd. This conclusion is further substantiated by examination of table 2 where the total positronium formation cross section has diminished to less than $10^{-3}\ \pi a_0^2$ at 20 Ryd. Another noteworthy aspect of table 1 is the fact that the UBA(3, 3) is clearly the superior perturbation theory when it comes to describing elastic scattering. While the UBA(3, 3) model is restricted to on-shell scattering, within that constraint the strong interaction between the positron and the proton requires a model that treats the e^+–p interaction (Walters 1984) higher than second order. It is worth noting that in an examination of elastic electron scattering from sodium it was similarly found that the on-shell unitarized distorted-wave

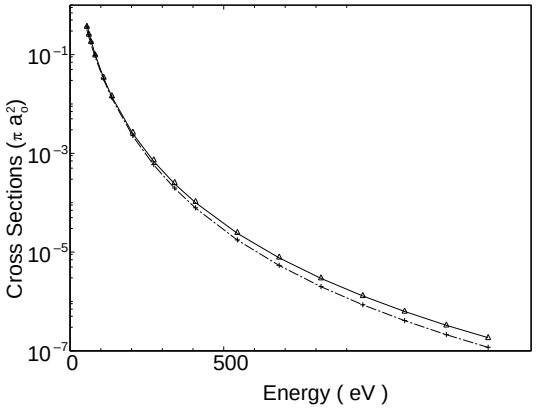

Figure 5. Cross sections (in πa_0^2) for positronium formation in the Ps(1s) state. The legend is the same as for figure 2.

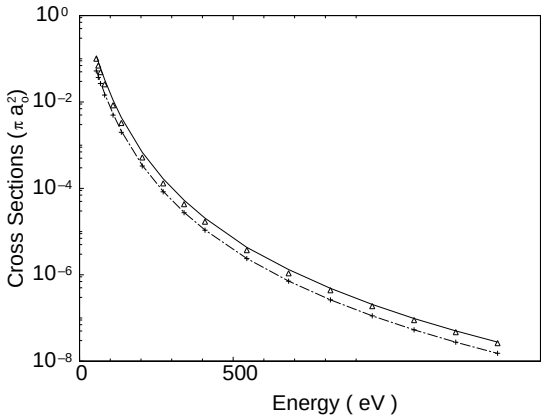

Figure 6. Cross sections (in πa_0^2) for positronium formation in the Ps(2s) state. The legend is the same as for figure 2.

Born approximation was superior to the off-shell distorted-wave second Born approximation (Bray *et al* 1989).

For the excitation processes to the H(2s) and H(2p) states, we also observe that the positronium channels have little effect for $E > 10$ Ryd (see figures 3 and 4) and that the inelastic cross section for the H(2p) state is an order of magnitude larger than the transition to the H(2s) state. At 5 Ryd, the CC(3, 3) model gave cross sections of 0.332, 0.0833 and 0.8284 πa_0^2 for the elastic, and inelastic excitation to the H(2s) and H(2p) states, respectively, and at 100 Ryd, the CC(3, 3) model gave cross sections of 0.0228, 0.004 59 and 0.1114 πa_0^2, respectively. For the H(2s) excitation, the perturbative methods do not show a reasonable agreement with the CC methods until $E > 80$ Ryd, and even then the SBA(3, 3), UBA(3, 3) and the FBA only converge at the 5% level. The small differences between the FBA and the CC models at low energies must be considered as fortuitous.

The transition to the H(2p) level is the only transition where the perturbative methods are in close agreement to each other as well as with the close-coupling methods at energies

Table 1. Total cross sections (in units of πa_0^2) for elastic scattering and excitation of H(2s) and H(2p) states at selected energies (in Ryd).

	Energy (Ryd)						
Model	5	10	20	40	60	80	100
H(1s) → H(1s)							
CC(3, 3)	0.3320	0.1890	0.1040	0.0548	0.0373	0.0283	0.0228
CC(3, 0)	0.2913	0.1812	0.1025	0.0547	0.0373	0.0283	0.0228
FBA	0.4275	0.2234	0.1142	0.0577	0.0386	0.0290	0.0232
SBA(3, 3)	0.5059	0.2429	0.1193	0.0591	0.0393	0.0294	0.0235
UBA(3, 3)	0.3341	0.1890	0.1030	0.0545	0.0371	0.0281	0.0227
H(1s) → H(2s)							
CC(3, 3)	0.0833	0.0516	0.0251	0.0120	0.784^{-2}	0.579^{-2}	0.459^{-2}
CC(3, 0)	0.1116	0.0543	0.0253	0.0120	0.784^{-2}	0.580^{-2}	0.460^{-2}
FBA	0.0830	0.0430	0.0219	0.0110	0.736^{-2}	0.552^{-2}	0.442^{-2}
SBA(3, 3)	0.1993	0.0754	0.0305	0.0133	0.842^{-2}	0.612^{-2}	0.480^{-2}
UBA(3, 3)	0.0621	0.0375	0.0204	0.0107	0.720^{-2}	0.544^{-2}	0.436^{-2}
H(1s) → H(2p)							
CC(3, 3)	0.8284	0.6231	0.3934	0.2341	0.1702	0.1346	0.1114
CC(3, 0)	0.9127	0.6313	0.3938	0.2341	0.1702	0.1346	0.1114
FBA	0.9316	0.6197	0.3868	0.2318	0.1691	0.1340	0.1111
SBA(3, 3)	0.9904	0.6606	0.4027	0.2365	0.1713	0.1353	0.1119
UBA(3, 3)	0.8362	0.5919	0.3791	0.2297	0.1682	0.1335	0.1107

Table 2. Total cross sections (in units of πa_0^2) for positronium formation in the Ps(1s), Ps(2s) and Ps(2p) levels at selected energies (in Ryd).

	Energy (Ryd)						
Model	5	10	20	40	60	80	100
H(1s) → Ps(1s)							
CC(3, 3)	0.1934	0.1390^{-1}	0.686^{-3}	0.240^{-4}	0.293^{-5}	0.626^{-6}	0.184^{-6}
FBA	0.1801	0.1348^{-1}	0.592^{-3}	0.177^{-4}	0.200^{-5}	0.410^{-6}	0.118^{-6}
SBA(3, 3)	0.1825	0.1460^{-1}	0.733^{-3}	0.249^{-4}	0.299^{-5}	0.632^{-6}	0.185^{-6}
UBA(3, 3)	0.1622	0.1289^{-1}	0.581^{-3}	0.175^{-4}	0.199^{-5}	0.408^{-6}	0.117^{-6}
H(1s) → Ps(2s)							
CC(3, 3)	0.0618	0.436^{-2}	0.167^{-3}	0.431^{-5}	0.485^{-6}	0.972^{-7}	0.277^{-7}
FBA	0.0267	0.200^{-2}	0.832^{-4}	0.237^{-5}	0.263^{-6}	0.533^{-7}	0.152^{-7}
SBA(3, 3)	0.0474	0.315^{-2}	0.126^{-3}	0.360^{-5}	0.423^{-6}	0.863^{-7}	0.253^{-7}
UBA(3, 3)	0.0290	0.212^{-2}	0.854^{-4}	0.239^{-5}	0.263^{-6}	0.533^{-7}	0.152^{-7}
H(1s) → Ps(2p)							
CC(3, 3)	0.785^{-2}	0.328^{-3}	0.180^{-4}	0.420^{-6}	0.386^{-7}	0.627^{-8}	0.149^{-8}
FBA	0.970^{-2}	0.414^{-3}	0.902^{-5}	0.129^{-6}	0.950^{-8}	0.144^{-8}	0.327^{-9}
SBA(3, 3)	0.1100	0.557^{-3}	0.229^{-4}	0.435^{-6}	0.371^{-7}	0.548^{-8}	0.135^{-8}
UBA(3, 3)	0.0148	0.618^{-3}	0.132^{-4}	0.176^{-6}	0.123^{-7}	0.180^{-8}	0.398^{-9}

$E > 20$ Ryd. Nevertheless, the UBA(3, 3) seems to slightly underestimate the cross section. At lower energies, as expected, the perturbative models do show differences with the CC models. It is also noticeable that the CC(3, 0) and CC(3, 3) model cross sections are quite different at the lower end of the energy scale.

The positronium-formation cross sections are given in table 2. As the energy increases,

the positronium-formation cross section in the Ps(1s) state increasingly dominates the total positronium-formation cross section. It is more than six times larger than the positronium cross section to the Ps(2s) state, which is in turn a factor of 10 larger than the positronium cross section to the Ps(2p) level. Inspection of figures 5–7 reveals that the Ps(2p) cross section is decreasing at a faster rate than the Ps(1s) and Ps(2s) cross sections. This is interesting since Shakeshaft and Wahedra (1980) predicted that at high energies the cross section for Ps-formation in $L = 1$ levels should be larger than the cross section in the Ps($L = 0$) levels.

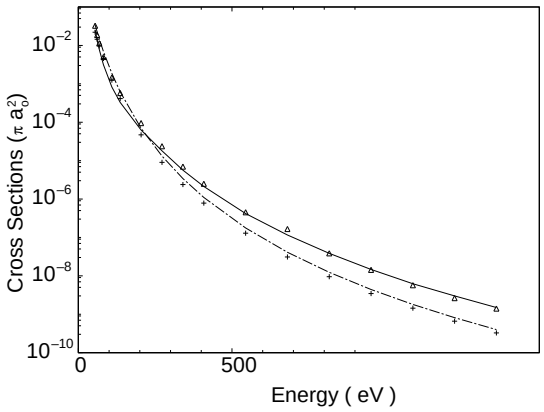

Figure 7. Cross sections (in πa_0^2) for positronium formation in the Ps(2p) state. The legend is the same as for figure 2.

We note the rapid decrease of the charge transfer process with energy as evidenced by table 2. At energies of 5 Ryd the charge exchange cross sections for Ps(1s), Ps(2s) are the same order of magnitude as those for excitation through the H(1s) and H(2s) states but thereafter they decrease more quickly. This is reflected by CC(3, 3) cross sections of 2.40^{-5}, 4.31^{-6} and 4.20^{-7} πa_0^2 for Ps(1s), Ps(2s) and Ps(2p) transitions, respectively, at 40 Ryd. The cross sections are even smaller at higher energies.

The other notable feature from table 2 and figures 5–7 is the failure of the on-shell FBA and UBA(3, 3) approximations to converge to the integrated cross section of the CC(3, 3) model. At the highest energy, the UBA(3, 3) cross section is 35% smaller that the CC(3, 3) cross section for the Ps(1s) transition. The agreement is even worse for the Ps(2s) and Ps(2p) transitions. Thus the fact that the FBA and UBA(3, 3) show reasonable agreement with CC(3, 3) cross sections for the 5 to 20 Ryd energy range must be considered as a fortuitous accident.

The SBA(3, 3) model on the other hand shows much better agreement with the CC(3, 3) model. At the highest energies, the agreement between the SBA(3, 3) and CC(3, 3) cross sections is at the 2% level. Differences are larger for the Ps(2s) and Ps(2p) cross sections, but at the highest energy, the SBA(3, 3) and CC(3, 3) are within 10% of each other. The superior quality of the agreement between them for the Ps(1s) transition can be explained by the nature of the positronium formation transition. The overlap of the H(1s) state with the Ps(1s) state is much larger than the overlap with the Ps(2s) and Ps(2p) states. Therefore, it is likely that higher-order processes are more important when the electron is being transferred to a Ps(2s) or Ps(2p) state. A conceivable reaction mechanism would be for the Ps($n = 2$) states to be populated by a transition from the Ps(1s) to Ps($n = 2$) states following a

second-order transition through the Ps(1s) state.

The conclusions to be drawn from table 2 and figures 5–7 are that an adequate description of the positronium-formation cross section cannot be gained from a model in which the scattering processes are restricted to remain on the energy shell. That the cross section for the SBA is consistently larger than the UBA and FBA cross sections provides strong evidence that off-shell scattering processes are a significant component of the reaction mechanism for the positronium formation transition.

Table 3. Partial cross sections (in units of πa_0^2) for e^+–H(1s) scattering at 10 Ryd.

	Final state					
J	H(1s)	H(2s)	H(2p)	Ps(1s)	Ps(2s)	Ps(2p)
0	0.0836	0.269^{-2}	0.781^{-4}	0.149^{-3}	0.377^{-4}	0.165^{-5}
1	0.0580	0.691^{-2}	0.321^{-2}	0.109^{-2}	0.307^{-3}	0.184^{-4}
2	0.0272	0.826^{-2}	0.707^{-2}	0.194^{-2}	0.569^{-3}	0.407^{-4}
3	0.0114	0.772^{-2}	0.0122	0.229^{-2}	0.695^{-3}	0.545^{-4}
4	0.445^{-2}	0.632^{-2}	0.0178	0.220^{-2}	0.688^{-3}	0.547^{-4}
5	0.170^{-2}	0.477^{-2}	0.0230	0.186^{-2}	0.596^{-3}	0.453^{-4}
6	0.678^{-3}	0.343^{-2}	0.0271	0.143^{-2}	0.469^{-3}	0.331^{-4}
7	0.319^{-3}	0.242^{-2}	0.0300	0.103^{-2}	0.344^{-3}	0.227^{-4}
8	0.198^{-3}	0.172^{-2}	0.0316	0.702^{-3}	0.239^{-3}	0.155^{-4}
9	0.154^{-3}	0.125^{-2}	0.0321	0.459^{-3}	0.159^{-3}	0.109^{-4}
10	0.133^{-3}	0.942^{-3}	0.0317	0.290^{-3}	0.102^{-3}	0.807^{-5}
Total	0.1885	0.0516	0.6231	0.0139	0.0044	0.000 33

The partial cross sections for all transitions from the H(1s) entrance channel at 10 Ryd are given in table 3. Note that the $J > 0$ partial cross sections are more dominant for the charge transfer processes, with the largest contribution coming from the $J = 3$ and 4. The positronium formation in the Ps(2p) state has the smallest flux loss and the positronium effects are becoming small (contributing about 2% of the total cross sections). For elastic scattering, the S-wave cross section is the largest, whereas for excitation to H(2s), the D-wave dominates. In the dipole excitation, the contributions from the larger partial waves dominate and a large number of partial waves need to be calculated to obtain a converged cross section.

We have also compared the cross sections from the present set of calculation with those from an earlier calculation (Mitroy and Stelbovics 1994) carried out with the CC(3, 3) model. At an energy of 4 Ryd, the integrated cross sections from the two calculations generally agree to within 5% with the exception being the cross section for H(2s) excitation for which we obtain 0.0888 πa_0^2 and which Mitroy and Stelbovics (1994) report as 0.0829 πa_0^2. As mentioned in the preceding section, the difficulties previously present in defining a particular grid to discretize the integral equation have now been overcome and the present calculations are expected to give cross sections which have a higher degree of numerical precision.

4. Cross sections for the Ps(1s) entrance channel

The integrated cross sections for elastic scattering, excitation of Ps(2s) and Ps(2p) states and the charge transfer transition to the H(1s), H(2s) and H(2p) hydrogen states when the entrance channel is Ps(1s) are shown in figures 8–13. Tabulated values of the cross sections

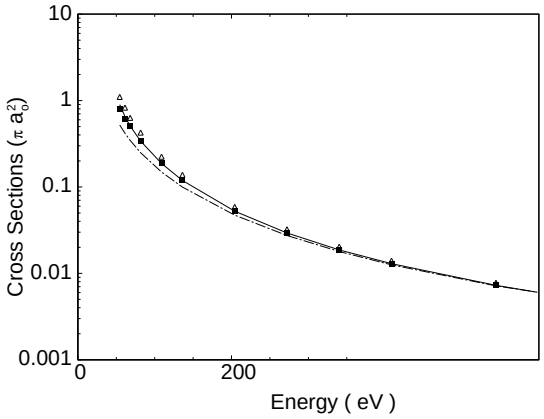

Figure 8. Cross sections (in πa_0^2) for elastic scattering of the Ps(1s) state. The cross sections are: CC(3, 3) (——), CC(0, 3) (□), UBA(3, 3) (— · —), FBA (+) and SBA(3, 3) (△).

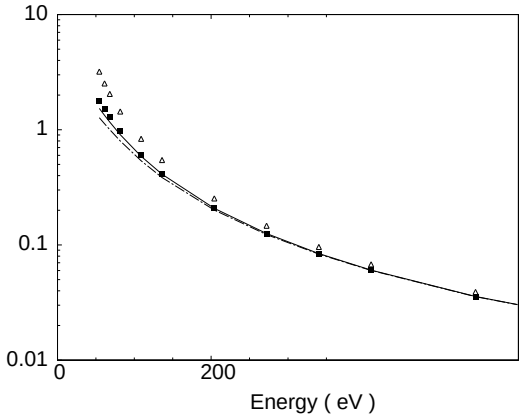

Figure 9. Cross sections (in πa_0^2) for excitation to the Ps(2s) state from the Ps(1s) entrance channel. The legend is the same as for figure 8.

are given for selected energies in tables 4 and 5. The energies listed in tables 4 and 5 and figures 8–13 are the energies in the e^+–H(1s) entrance channel. The energy in the Ps(1s)–p entrance channel is 0.5 Ryd smaller.

The elastic scattering for the Ps(1s) channel has an interesting feature in that the FBA to the elastic T-matrix element is zero. This is a trivial consequence of the fact that the centre of the charge distribution and the centre of the mass are located at the same point (Massey and Mohr 1954). All the FBA matrix elements which connect positronium states of the same parity can be shown to vanish (see, for example, Mitroy 1993c, Au 1985) Hence, elastic scattering occurs as a result of second- and higher-order processes. In contrast to the trends at low energy (Mitroy and Stelbovics 1994), elastic scattering does not dominate the scattering process at high energies. From table 4, it can be seen that the CC(3, 3) and CC(0, 3) elastic cross sections are less than 1% different for energies greater than 20 Ryd. Therefore, we conclude that the rearrangement kernel exerts a negligible effect upon positronium elastic

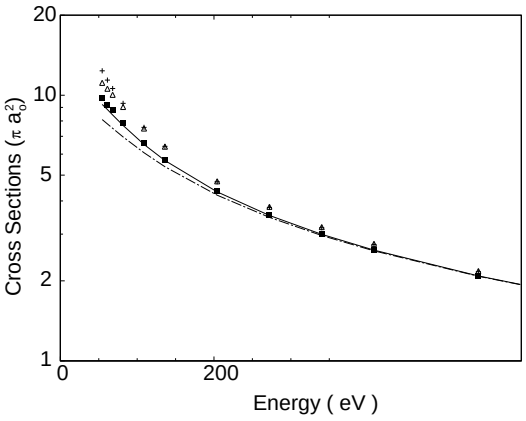

Figure 10. Cross sections (in πa_0^2) for excitation to the Ps(2p) state from the Ps(1s) entrance channel. The legend is the same as for figure 8.

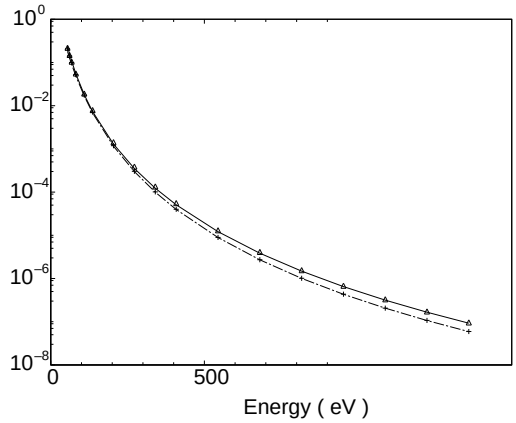

Figure 11. Cross sections (in πa_0^2) for hydrogen formation in the H(1s) state. The legend is the same as for figure 8.

scattering for energies greater than 20 Ryd. The SBA$(3, 3)$ has converged to the 5% level of accuracy for $E \geqslant 40$ Ryd.

For the excitation processes to the Ps(2s) and Ps(2p) states, we also observe that the hydrogen channels have little effect for $E > 10$ Ryd (see figures 9 and 10). As was the case for elastic scattering, the CC$(3, 3)$ and CC$(0, 3)$ show near perfect agreement for energies greater than 20 Ryd. There is no cross section given for the Ps(1s)–Ps(2s) transition for the FBA since it is identically zero. It is worth noting that the UBA$(3, 3)$ gives an excellent description of the Ps(2s) and Ps(2p) excitation process (see table 4) for $E > 20$ Ryd. For the Ps(1s)–Ps(2p) transition, the FBA is non-zero since the initial and final Ps states have opposite parity. All of the perturbation theory results converge slowly towards the CC$(3, 3)$ cross sections as the energy increases. We note that the FBA converges to the SBA$(3, 3)$ at $E > 20$ Ryd and both these models tend to converge to the CC$(3, 3)$ at high energies. The transition to the Ps(2p) level is the largest single cross section at all energies considered and increasingly dominates the scattering process as the energy gets larger. The

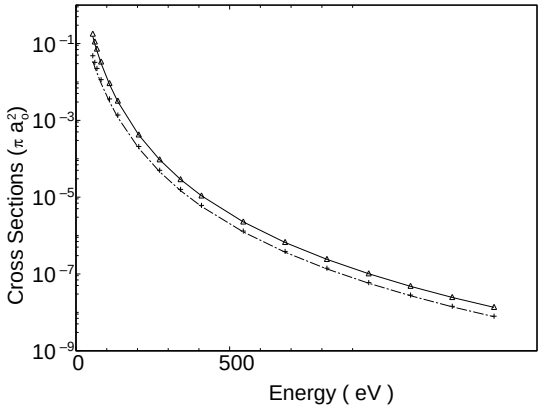

Figure 12. Cross sections (in πa_0^2) for hydrogen formation in the H(2s) state. The legend is the same as for figure 8.

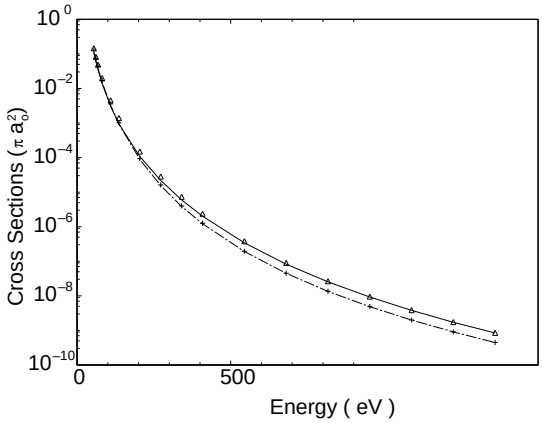

Figure 13. Cross sections (in πa_0^2) for hydrogen formation in the H(2p) state. The legend is the same as for figure 8.

$p + Ps(1s) \rightarrow p + Ps(nl)$ cross sections are much larger than the corresponding positron–hydrogen transitions. This is due to the larger size of the Ps atom.

The hydrogen formation cross sections are given in table 5. For the charge transfer process, the capture to the H(1s) state dominates the scattering process at all the energies considered. Capture to the H(2p) state is less important; for example, at 100 Ryd, the CC(3, 3) gives cross sections of 9.26^{-8}, 1.35^{-8} and 8.46^{-10} πa_0^2 for the electron capture to the 1s, 2s and 2p levels, respectively. In general, it can be seen from figures 11–13, that there is a distinct difference between the behaviour of the SBA(3, 3) and the on-shell UBA(3, 3) and FBA models as the energy increases. While the SBA(3, 3) converges to the CC(3, 3) cross sections, the UBA(3, 3) converges to the FBA. Although the cross sections are very small, the differences between the off-shell and on-shell models can be as large as 50% for $E > 60$ Ryd. These large differences at high energies once again suggest that the off-shell effects are extremely important in describing the scattering process for rearrangement transitions.

Table 4. Total cross sections (in units of πa_0^2) for elastic scattering and excitation of Ps(2s) and Ps(2p) states at selected energies. The energy is the energy in the e^+–H(1s) entrance channel.

	Energy (Ryd)						
Model	5	10	20	40	60	80	100
Ps(1s) → Ps(1s)							
CC(3, 3)	0.5068	0.1190	0.0293	0.728^{-2}	0.323^{-2}	0.181^{-2}	0.115^{-2}
CC(0, 3)	0.4870	0.1227	0.0293	0.734^{-2}	0.323^{-2}	0.181^{-2}	0.115^{-2}
SBA(3, 3)	0.6201	0.1361	0.0318	0.765^{-2}	0.335^{-2}	0.186^{-2}	0.118^{-2}
UBA(3, 3)	0.3462	0.0996	0.0274	0.717^{-2}	0.321^{-2}	0.181^{-2}	0.118^{-2}
Ps(1s) → Ps(2s)							
CC(3, 3)	1.1660	0.4113	0.1256	0.0357	0.0167	0.964^{-2}	0.626^{-2}
CC(0, 3)	1.2740	0.4176	0.1260	0.0357	0.0167	0.964^{-2}	0.626^{-2}
SBA(3, 3)	2.0200	0.5391	0.1450	0.0386	0.0176	0.100^{-2}	0.646^{-2}
UBA(3, 3)	1.0020	0.3849	0.1231	0.0356	0.0167	0.964^{-2}	0.626^{-2}
Ps(1s) → Ps(2p)							
CC(3, 3)	8.426	5.677	3.527	2.087	1.488	1.146	0.921
CC(0, 3)	8.570	5.747	3.529	2.085	1.488	1.146	0.921
FBA	10.600	6.418	3.781	2.167	1.526	1.166	0.933
SBA(3, 3)	9.983	6.366	3.779	2.167	1.526	1.166	0.933
UBA(3, 3)	7.505	5.380	3.469	2.081	1.488	1.146	0.921

Table 5. Total cross sections (in units of πa_0^2) for hydrogen formation in the H(1s), H(2s) and H(2p) states at selected energies. The energy is the energy in the e^+–H(1s) entrance channel.

	Energy (Ryd)						
Model	5	10	20	40	60	80	100
Ps(1s) → H(1s)							
CC(3, 3)	0.1075	0.729^{-2}	0.352^{-3}	0.121^{-4}	0.148^{-5}	0.315^{-6}	0.926^{-7}
FBA	0.1000	0.710^{-2}	0.304^{-3}	0.895^{-5}	0.101^{-5}	0.206^{-6}	0.592^{-7}
SBA(3, 3)	0.1014	0.767^{-2}	0.376^{-3}	0.126^{-4}	0.151^{-5}	0.318^{-6}	0.929^{-7}
UBA(3, 3)	0.0901	0.678^{-2}	0.298^{-3}	0.887^{-5}	0.100^{-5}	0.205^{-6}	0.589^{-7}
Ps(1s) → H(2s)							
CC(3, 3)	0.0649	0.307^{-2}	0.941^{-4}	0.226^{-5}	0.240^{-6}	0.478^{-7}	0.135^{-7}
FBA	0.0226	0.138^{-2}	0.501^{-4}	0.131^{-5}	0.141^{-6}	0.281^{-7}	0.793^{-8}
SBA(3, 3)	0.0713	0.314^{-2}	0.930^{-4}	0.223^{-5}	0.237^{-6}	0.472^{-7}	0.133^{-7}
UBA(3, 3)	0.0173	0.119^{-2}	0.459^{-4}	0.124^{-5}	0.135^{-6}	0.272^{-7}	0.770^{-8}
Ps(1s) → H(2p)							
CC(3, 3)	0.0352	0.947^{-3}	0.219^{-4}	0.342^{-6}	0.253^{-7}	0.380^{-8}	0.846^{-9}
FBA	0.0432	0.103^{-2}	0.162^{-4}	0.196^{-6}	0.136^{-7}	0.200^{-8}	0.447^{-9}
SBA(3, 3)	0.0471	0.134^{-2}	0.273^{-4}	0.365^{-6}	0.254^{-7}	0.371^{-8}	0.814^{-9}
UBA(3, 3)	0.0377	0.941^{-3}	0.155^{-4}	0.192^{-6}	0.135^{-7}	0.199^{-8}	0.446^{-9}

The partial cross sections for all transitions from the Ps(1s) entrance channel at 10 Ryd are given in table 6. It is evident that the larger partial waves are contributing significantly to the elastic scattering and excitation to Ps(2s) and Ps(2p) states. The partial cross sections are still increasing at $J = 10$. This a manifestation of the larger size of the Ps atom as compared with the hydrogen atom.

Table 6. Partial cross sections (in units of πa_0^2) for Ps(1s)–p scattering at 10 Ryd.

	Final state					
J	H(1s)	H(2s)	H(2p)	Ps(1s)	Ps(2s)	Ps(2p)
0	0.783^{-4}	0.508^{-4}	0.185^{-4}	0.283^{-4}	0.697^{-4}	0.133^{-2}
1	0.572^{-3}	0.249^{-3}	0.427^{-4}	0.227^{-3}	0.149^{-3}	0.602^{-2}
2	0.102^{-2}	0.425^{-3}	0.679^{-4}	0.569^{-3}	0.298^{-3}	0.0159
3	0.121^{-2}	0.496^{-3}	0.870^{-4}	0.111^{-2}	0.610^{-3}	0.0317
4	0.116^{-2}	0.475^{-3}	0.977^{-4}	0.192^{-2}	0.117^{-2}	0.0520
5	0.978^{-3}	0.402^{-3}	0.101^{-3}	0.299^{-2}	0.206^{-2}	0.0749
6	0.753^{-3}	0.312^{-3}	0.987^{-4}	0.420^{-2}	0.330^{-2}	0.0977
7	0.541^{-3}	0.227^{-3}	0.912^{-4}	0.536^{-2}	0.488^{-2}	0.1187
8	0.369^{-3}	0.157^{-3}	0.802^{-4}	0.631^{-2}	0.673^{-2}	0.1366
9	0.242^{-3}	0.104^{-3}	0.672^{-4}	0.696^{-2}	0.874^{-2}	0.1507
10	0.153^{-3}	0.665^{-4}	0.539^{-4}	0.730^{-2}	0.0108	0.1609
Total	0.729^{-2}	0.306^{-2}	0.947^{-3}	0.1190	0.4113	5.6770

5. Differential cross sections

In this section differential cross sections for elastic positron–hydrogen scattering (figure 14(*a*)), positronium formation in the ground state (figure 14(*b*)), and elastic scattering for the Ps(1s)–p entrance channel (figure 14(*c*)) are reported. While there have been no experimental measurements of differential cross sections (DCS) for positron–hydrogen scattering, examination of the DCS can be used to deduce information about the reaction mechanism through the comparison of the different model cross sections with each other. The calculation of the differential cross section at high energy requires increased care with regard to the convergence of the partial-wave sum.

The computation of the DCS for positronium formation was relatively easy since the positronium formation matrix element is a short-range matrix element and decays quickly as J increases. The full CC equations were solved with explicit inclusion of Ps formation for $J \leqslant 26$. Decoupled CC equations were solved up to $J \leqslant 80$ and the UBA was used for $80 < J \leqslant 400$. The partial-wave sum was extended to $J = 400$ by the need to obtain smooth cross sections for Ps–p scattering. At the changeover from the CC to the UBA it was noticeable that the real part of the elastic CC T-matrix elements for e^+–H(1s) and Ps(1s)–p scattering was essentially identical to the SBA and the imaginary part of the CC T-matrix elements was almost equal to the UBA.

Beyond $J > 80$ special procedures were introduced to compute the real parts of the elastic scattering T-matrix element for the CC and SBA models. As it is known that the phase shift scales like J^{-3} in the adiabatic polarization formula, the real part of the T-matrix elements was computed for $J > 80$ by assuming the T-matrix elements scaled like J^{-3}. The UBA was used to compute the imaginary part of the T-matrix element for > 80.

Figure 14(*a*) depicts the DCS for e^+–H(1s) in the CC(3, 3), CC(3, 0), UBA(3, 3) and SBA(3, 3) approximations. All the approximations seem to predict roughly the same shape for the DCS with minor differences at small and large angles. The almost perfect agreement between the CC(3, 3) and CC(0, 3) differential cross sections indicates that positronium formation has almost no influence on elastic positron–hydrogen scattering for energies of 10 Ryd or greater. This is to be expected at a high energy like 10 Ryd. It is noticeable that the UBA(3, 3) tends to a factor of two different from the CC(3, 3) DCS section at small angles and the SBA(3, 3) overestimates the CC(3, 3) DCS at large angles. Scattering at small

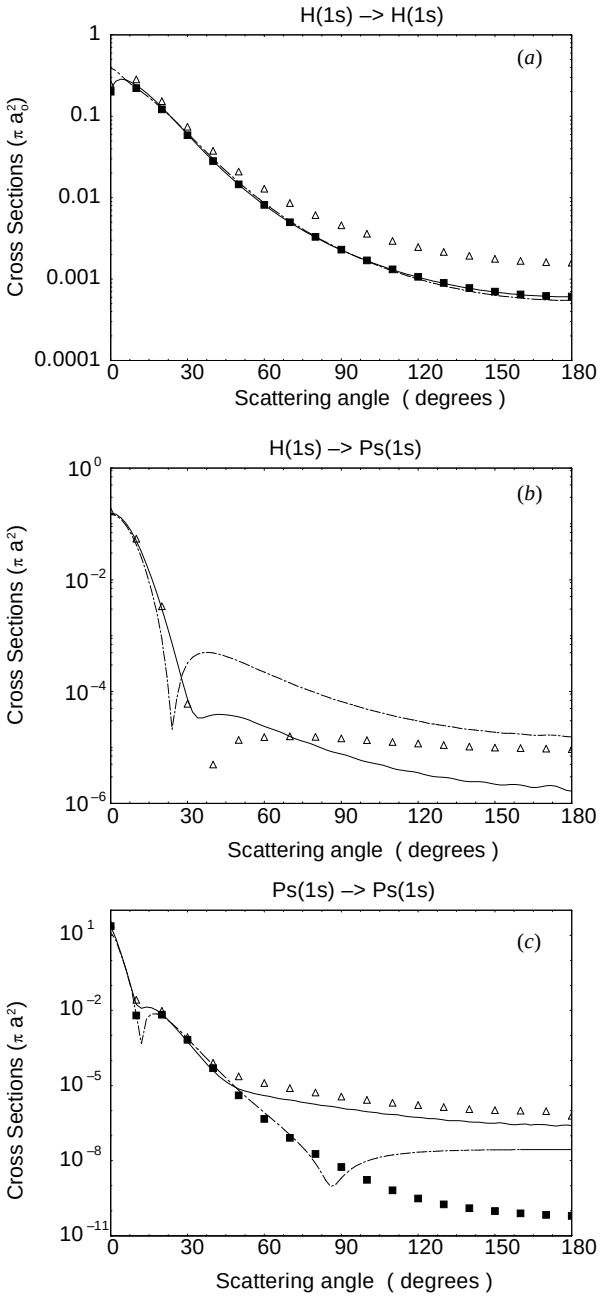

Figure 14. The differential cross sections for e^+–H elastic scattering (*a*), positronium formation (*b*), and Ps(1s)–p elastic scattering (*c*) (in a_0^2). The cross sections are: CC(3, 3) (——), CC(3, 0) or CC(0, 3) (□), UBA(3, 3) (— · —), and SBA(3, 3) (△).

angles is heavily influenced by polarization effects and off-shell processes need to be taken into consideration (e.g. as described in the previous paragraph, the SBA(3, 3) is a much better approximation to the CC(3, 3) T-matrix element at high J than is the UBA(3, 3)).

Large-angle scattering is dominated by the strong positron–hydrogen interaction and third- and higher-order processes can have a significant influence. While the UBA(3, 3) model restricts all scattering events to remain on the energy shell, it does treat the interaction between the positron and nucleus to all orders of perturbation theory and so does a better job of reproducing the CC(3, 3) DCS than the SBA(3, 3) model.

One of the unusual features of figure 14(*a*) is the dip in the DCS for forward scattering. An examination of the phase shifts reveals that the phase is negative for $J < 10$ and positive for $J \geqslant 10$. This is to be expected since large-angle scattering will be dominated by the repulsive interaction between the positron and the proton while small-angle scattering is expected to be dominated by the attractive polarization potential. The destructive interference between the different partial waves leads to the dip in the DCS at 0°. We have examined other calculations of e^+–H DCS (Sarkar and Ghosh 1994, Walters 1988) and not observed a dip in the forward angle cross section. We suspect these other groups did not observe the dip because they did not go to the same lengths to get accurate T-matrix elements at the higher partial waves.

The DCS for Ps(1s) formation is shown in figure 14(*b*). The CC(3, 3) has a very shallow minimum at around 30° and a very weak secondary maximum near 50°. Both the UBA(3, 3) and SBA(3, 3) models do a reasonable job of reproducing the CC(3, 3) DCS at forward angles. At backward angles neither model is particularly good but the SBA(3, 3) provides a marginally superior representation of the CC(3, 3) DCS.

The Ps(1s)–p elastic DCS for the CC(3, 3), CC(0, 3), SBA(3, 3) and UBA(3, 3) models are shown in figure 14(*c*). The CC(3, 3) and SBA(3, 3) models possess a shoulder near 10°, while the CC(0, 3) and UBA(3, 3) show a pronounced dip at this angle. The CC(3, 3) and SBA(3, 3) DCS are both relatively flat at the higher angles with the SBA(3, 3) DCS being slightly larger than the CC(3, 3) cross section. This provides evidence that elastic scattering in the Ps(1s)–p entrance channel is primarily a second-order process. Of particular importance is the small size of the cross section at backward angles. The CC(3, 3) and SBA(3, 3) cross sections are about $10^{-6}\ a_0^2$ at 180°. This is about 300 times smaller than the DCS for elastic e^+–H(1s) scattering. This is not surprising since there is no electrostatic interaction between the proton and the positronium to cause backward scattering. The differences between the CC(3, 3) and CC(0, 3) cross section at backward angles indicate that the rearrangement channels have an influence on the Ps–p elastic scattering process. The absence of an electrostatic interaction makes the elastic Ps–p DCS much more sensitive to second-order processes involving positronium formation and this is reflected in the large difference between the CC(3, 3) and CC(0, 3) DCS. All three models allowing for off-shell scattering predict roughly the same size DCS in the forward direction. The UBA(3, 3) model gives a forward angle cross section which is some 40% smaller than the CC(3, 3) DCS.

6. Phase shifts for e^+–H(1s) and Ps(1s)–p scattering

In figures 15(*a*) and 16(*a*), the real part of the $J = 0$, 1 and 2 elastic phase shifts for the positron–hydrogen and positronium–proton entrance channels, respectively, are depicted. The differences between the two sets of phase shifts could hardly be greater. The positron–hydrogen phase shifts decrease very slowly while the elastic positronium–proton phase shifts fall rapidly towards zero. Mitroy *et al* (1995) looked at the phase shifts and gave the following estimates for the behaviour of the phase shifts at high energies. In the case of positron–hydrogen scattering, the phase shifts decrease as $O(\ln k/k)$. The rapid decrease of the elastic positronium–proton phase shifts was attributed to the absence of the first-order term in the Ps(1s)–p elastic scattering and the high-energy behaviour of the phase shifts

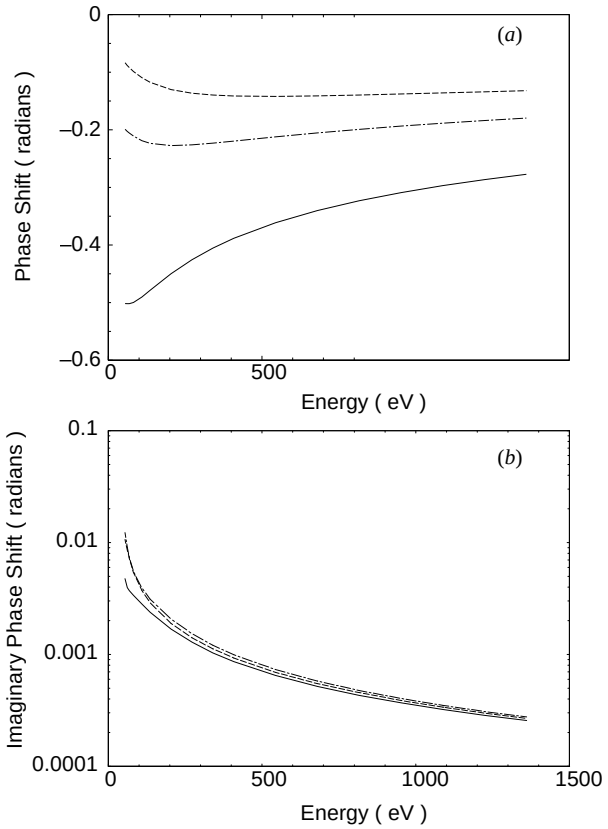

Figure 15. The real (*a*) and imaginary (*b*) elastic phase shifts for e^+–H scattering as computed in the CC(3, 3) model. The curves are for $L = 0$ (——), $L = 1$ (— · —) and $L = 2$ (– – –).

was noted as $O(1/k^3)$. For completeness, the imaginary parts of the phase shifts are shown in figures 15(*b*) and 16(*b*). There is no fundamental and qualitative difference between the two plots of the imaginary part of the phase shift. The imaginary part of the phase shift is related to the excitation cross section, and for both the e^+–H(1s) and Ps(1s)–p entrance channels the dominant excitation at high energies is the dipole excitation. Therefore it is to be expected that both entrance channels exhibit a similar asymptotic form for the imaginary part of the phase shift. In this section, we give details of the analysis leading to those conclusions.

We begin by observing the behaviour of the elastic scattering phase shifts for a suitably well behaved local potential $V(r)$, as the incident momentum k goes to infinity, is given in the Born approximation (Newton 1982) as

$$\delta_L = \frac{1}{2k}\int_0^\infty \mathrm{d}r\, V(r) \tag{4}$$

and thus $\delta_L \sim O(1/k)$ as $k \to \infty$. Unfortunately for e^+–H(1s) elastic scattering, the static potential $V(r) = (1 + 1/r)e^{-2r}$ is singular at the origin and hence the Born phase shifts cannot be found from (4). In this case the FBA amplitude is

$$f_B(\boldsymbol{k}, \boldsymbol{k}') = -2\frac{|\boldsymbol{k} - \boldsymbol{k}'|^2 + 8}{(|\boldsymbol{k} - \boldsymbol{k}'|^2 + 4)^2} \tag{5}$$

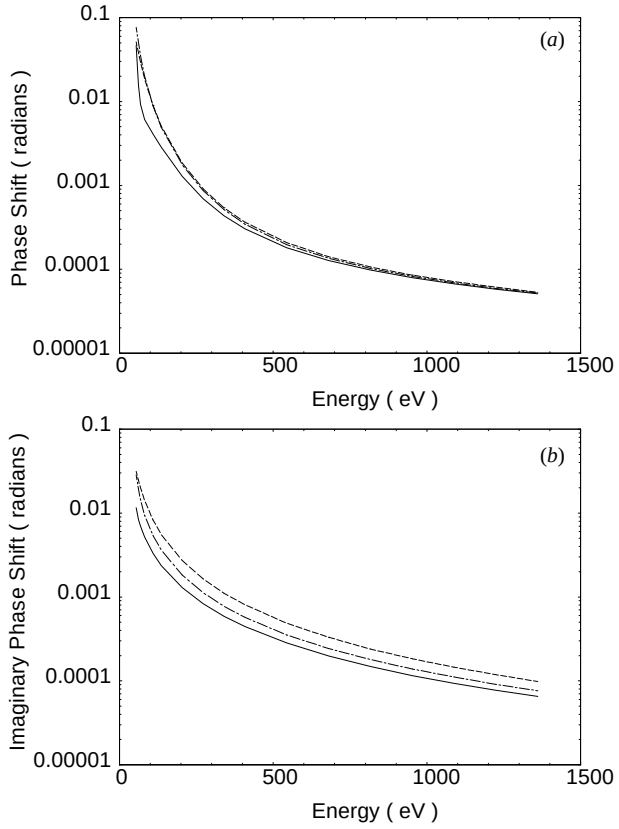

Figure 16. The absolute value of the real (*a*) and imaginary (*b*) elastic phase shifts for Ps(1s)–p scattering as computed in the CC(3, 3) model. The legend is the same as for figure 15.

and after expanding in a partial-wave expansion the Born phase shifts are given as

$$\delta_{lB} = \frac{1}{k}\left[1 - \frac{l\alpha}{2(1+\alpha)}\,Q_l(\alpha) + \frac{l}{2(l+\alpha)}\,Q_{l-1}(\alpha)\right] \sim \frac{\ln k}{k} \tag{6}$$

where $\alpha = 1 + 2/k^2$. It is apparent from figure 15 that the phase shifts approach the common asymptote independent of l very slowly with increasing energy.

In the positronium–proton elastic scattering, the FBA matrix element, i.e. $\langle \boldsymbol{k}'\Phi_{1s}|V|\boldsymbol{k}''\Phi_{1s}\rangle = 0$ as already noted. The lack of a first-order term for this particular channel means the scattering phase shifts at high energies are dominated by the second Born term. The leading term to the elastic T-matrix element for positronium–proton scattering can be written as

$$\langle \boldsymbol{k}'\Phi_{1s}|T|\boldsymbol{k}\Phi_{1s}\rangle \sim \int \mathrm{d}^3q\, \frac{\langle \boldsymbol{k}'\Phi_{1s}|V|\boldsymbol{q}\Phi_{2p}\rangle\langle \boldsymbol{q}\Phi_{2p}|V|\boldsymbol{k}\Phi_{1s}\rangle}{(E^{(+)} - \varepsilon_{2p} - \frac{1}{4}q^2)}. \tag{7}$$

It has been confirmed numerically that the coupling to the hydrogenic intermediate states is negligible when compared to the Ps(2p) intermediate state. At 100 Ryd, we found that the Ps(2p) intermediate state contributed as much as 99% of the second-Born T-matrix element.

There is, of course, no contribution to the second-order T-matrix from the intermediate Ps(1s) and Ps(2s) since those matrix elements are zero by the parity selection rules. A partial-wave analysis of this integral by purely algebraic means and a subsequent analysis of the high momentum limit for general J proved to be an extremely formidable proposition and our attempts at a completely algebraic solution failed. The difficulty in finding a general analytic form for the SBA at non-zero momentum transfer has been noted previously (Walters 1984). However, we can draw some conclusions for the $J = 0$ partial wave. We can show that the partial-wave first-order term for $J = 0$ can be written as

$$\langle \boldsymbol{q}\Phi_{2p}|V|\boldsymbol{k}\Phi_{1s}\rangle^{J=0} = \frac{24}{\sqrt{2\pi}}\left(\frac{q^2-k^2}{2q^2}I_1 - I_2\right) \tag{8}$$

where

$$I_1 = \frac{1}{2k}\left[\frac{2}{9}\left(\frac{1}{((q+k)^2+\frac{9}{4})^2} - \frac{1}{((q-k)^2+\frac{9}{4})^2}\right) + \frac{16}{81}\left(\frac{1}{(q+k)^2+\frac{9}{4}} - \frac{1}{(q-k)^2+\frac{9}{4}}\right) - \frac{64}{243}\left(\ln\frac{(q+k)^2+\frac{9}{4}}{(q-k)^2+\frac{9}{4}} - \ln\frac{(q-k)^2}{(q+k)^2}\right)\right] \tag{9}$$

$$I_2 = \frac{1}{8kq^2}\left(\frac{1}{(q+k)^2+\frac{9}{4}} - \frac{1}{(q-k)^2+\frac{9}{4}}\right). \tag{10}$$

The second Born term, $T_{SBA}^{J=0}(1s, 1s)$ can then be evaluated by

$$T_{SBA}^{J=0}(1s, 1s) = \int_0^\infty dq\, \frac{q^2\langle \boldsymbol{k}\Phi_{1s}|V|\boldsymbol{q}\Phi_{2p}\rangle^0\langle \boldsymbol{q}\Phi_{2p}|V|\boldsymbol{k}\Phi_{1s}\rangle^0}{(E^{(+)} - \varepsilon_{2p} - \frac{1}{4}q^2)}. \tag{11}$$

The real part of the T_{SBA} is the principal value of the above integral and the imaginary part is simply

$$\mathrm{Im}(T_{SBA}^0) = -2\pi k(\langle \boldsymbol{k}\Phi_{1s}|V|\boldsymbol{k}'\Phi_{2p}\rangle^0)^2 \tag{12}$$

where k, k' are the on-shell momenta in the respective channels. It is straightforward but tedious to obtain the partial-wave matrix elements and thus determine the leading high-momentum term. It is

$$\mathrm{Im}(T_{SBA}) \sim \frac{4096}{6561}\frac{(\ln k)^2}{k^5}. \tag{13}$$

The real part of the $J = 0$ T-matrix can be reduced to a one-dimensional non-singular integral. The integrand contains a class of logarithmic functions which cannot be evaluated analytically. We therefore resorted to a numerical integration of equation (12) to find the asymptotic power law. The numerical integration was performed using a composite Gaussian mesh totalling some 70 000 points and utilized quadruple (128 bit) precision arithmetic. Explicit numerical calculations of the second Born approximation have been performed at energies up to and including 10^8 Ryd. By examining the behaviour of the T-matrix element, we were able to determine that the

$$\mathrm{Re}(T_{SBA}^0) \sim \frac{0.175}{k^4}. \tag{14}$$

Converting the T-matrix to a phase shift by

$$\mathrm{Re}(\delta_0) = -\frac{1}{2}\tan^{-1}\left(\frac{-4\pi k\,\mathrm{Re}(T_{SBA})}{1+4\pi k\,\mathrm{Im}(T_{SBA})}\right) \tag{15}$$

and noting that the imaginary T-matrix element decreases more rapidly than the real one, the leading-order term in the high-energy expression for the real phase shift is

$$\delta_0^R \sim \frac{1.10}{k^3}. \tag{16}$$

The analytic result for the imaginary T-matrix was also verified numerically to check the fitting procedure used in finding the leading term of the real T-matrix. The energy dependence of the imaginary T-matrix elements are consistent with the asymptotic forms, at the highest energy of 10^8 Ryd, the asymptotic and numerical T-matrix elements agree to within 2%. The results of the simplified second Born analysis have also been verified to be a reasonably accurate approximation to the full solution of the Lippmann–Schwinger equation for the CC(3, 3) model. At an energy of 200 Ryd, there is only a 5% difference between the two results. A similar behaviour for higher partial waves can be inferred from our $J = 0$ results as is clear from the $J = 1, 2$ partial waves in figure 15(a).

7. Conclusions

In this work, a comprehensive set of calculations for e^+–H and Ps–p scattering at energies ranging from 4–100 Ryd has been performed. Cross sections and phase shifts have been calculated using the CC(3, 3), CC(3, 0), CC(0, 3), FBA, SBA and UBA(3, 3) models. The present six-state basis includes most of the physical reaction mechanism and complexities of a larger-scale calculation. Therefore it is expected that the conclusions will have a general validity.

By comparing the integrated cross sections for the CC(3, 3) model with those of the CC(0, 3) and CC(3, 0) models we observed that the positronium channels have little effect on the $e^+ + H(1s) \rightarrow e^+ + H(nl)$ processes at $E > 15$ Ryd. Similarly, the hydrogen channels have negligible effect on the $Ps(1s) + p \rightarrow Ps(nl) + p$ processes for $E > 15$ Ryd. We conclude that it is possible to describe the direct reaction channels of the positron–hydrogen system to good accuracy using models that only include one manifold of states and do not admit the possibility of rearrangement collisions for energies greater than 15 Ryd.

The ability of the different varieties of perturbation theory to give a reliable estimate of the fully coupled solution of the Lippmann–Schwinger equation depended on the nature of the collision. Broadly speaking, all the approximations tested, FBA, UBA and SBA, were reasonably accurate for the direct transitions not involving an electron transfer (with the exception of Ps(1s)–p elastic scattering) and gave integrated cross sections which were within 5% of the CC(3, 3) cross section at 100 Ryd. However, this was not the case for the rearrangement collisions. The on-shell approximations did a uniformly poor job of reproducing the CC(3, 3) cross sections. At 100 Ryd, the UBA cross sections are roughly half the size of the CC(3, 3) cross sections. The SBA does a better job and in the worst case is no more than 10% different from the CC(3, 3) cross section. This provides strong evidence that off-shell scattering processes play a strong part in the electron transfer reaction even at high energies.

Elastic scattering in the Ps(1s)–p entrance channel is seen to be very unusual and as far as we are aware there is no other quantum collision system (apart from analogues like μ_-, μ_+, p) that behaves in a similar fashion. The lack of a first-order interaction results in a set of phase shifts that decrease more rapidly than those of any other quantum system. In this respect, the Ps(1s)–p system may be said to be unique.

Acknowledgments

KR would like to acknowledge the hospitality provided by the Centre of Atomic, Molecular and Surface Physics (CAMSP), as well as Dr Lindsay Berge for assistance in using the computing facilities at the Centre. Most of the calculations were done on a SUN10/52 model at the Computing Services Unit, University of Malaya and the analyses were carried out on the IBM RS6000/32H at CAMSP.

References

Basu D, Banerji G and Ghosh A S 1976 *Phys. Rev.* A **13** 1381
Basu M and Ghosh A S 1988 *J. Phys. B: At. Mol. Opt. Phys.* **21** 3439–47
Bhatia A K, Temkin A, Drachman R J and Eiserike H 1971 *Phys. Rev.* A **3** 1328
Bhatia A K, Temkin A and Eiserike H 1974 *Phys. Rev.* A **9** 219
Bransden B H 1969 *Case. Stud. At. Collision Phys.* **1** 171
Bransden B H, McCarthy I E and Stelbovics A T 1985 *J. Phys. B: At. Mol. Phys.* **18** 823
Bransden B H and Noble C J 1994 *Adv. At. Mol. Phys.* **32** 19–37
Bray I, McCarthy I E, Mitroy J and Ratnavelu K 1989 *Phys. Rev.* A **39** 4998
Burke P G, Schey H M and Smith K 1963 *Phys. Rev.* A **129** 1258
Ghosh A S and Darewych J W 1991 *J. Phys. B: At. Mol. Opt. Phys.* **24** L629
Ghosh A S, Sil N C and Mandal P 1982 *Phys. Rep.* **87** 313
Hewitt N R, Noble C J and Bransden B H 1990 *J. Phys. B: At. Mol. Opt. Phys.* **23** 4185
Higgins K, Burke P G and Walters H R J 1990 *J. Phys. B: At. Mol. Opt. Phys.* **23** 1345
Humberston J W 1982 *Can. J. Phys.* **60** 591
——1984 *J. Phys. B: At. Mol. Phys.* **17** 2353
Jones G O, Charlton M, Slevin J, Larricchia G, Kover A, Poulsen M R and Nic Chormaic S 1993 *J. Phys. B: At. Mol. Opt. Phys.* **26** L483
Kernoghan A A, McAlinden M T and Walters H R J 1995 *J. Phys. B: At. Mol. Opt. Phys.* **28** 1079
McAlinden M T, Kernoghan A A and Walters H R J 1994 *Hyperfine Interact.* **89** 161
McCarthy I and Stelbovics A T 1983 *Phys. Rev.* A **28** 2693
Mitroy J 1993a *J. Phys. B: At. Mol. Opt. Phys.* **26** L625–31
——1993b *J. Phys. B: At. Mol. Opt. Phys.* **26** 4861–9
——1993c *Aust. J. Phys.* **46** 751–71
——1995 *Aust. J. Phys.*
Mitroy J, Berge L and Stelbovics A T 1994 *Phys. Rev. Lett.* **73** 2966–70
Mitroy J and Ratnavelu K 1995 *J. Phys. B: At. Mol. Opt. Phys.* **27** 1–20
Mitroy J, Ratnavelu K and Stelbovics A T 1995 *Phys. Rev. Lett.*
Mitroy J and Stelbovics A T 1994 *J. Phys. B: At. Mol. Opt. Phys.* **27** 3257–75
Morgan L A 1982 *J. Phys. B: At. Mol. Phys.* **15** L25
Sarkar N K and Ghosh A S 1994 *J. Phys. B: At. Mol. Opt. Phys.* **27** 759
Shakeshaft R and Wahedra J M 1980 *Phys. Rev.* A **22** 968–75
Sperber W, Becker D, Lynn K G, Raith W, Schwab A, Sinapius G, Spicher G and Weber M 1992 *Phys. Rev. Lett.* **68** 3690–2
Spicher G, Olsson B, Raith W, Sinapius G and Sepber W 1990 *Phys. Rev. Lett.* **64** 1019
Walters H R J 1984 *Phys. Rep.* **116** 1
——1988 *J. Phys. B: At. Mol. Opt. Phys.* **21** 1893
Weber M, Hofmann A, Sperber W, Jacobsen F M and Lynn K G 1994 *Hyperfine Interact.* **89** 221–4
Zhou S, Kauppila W E, Kwan C K and Stein T S 1994 *Phys. Rev. Lett.* **72** 1443